中国光学（中英文） Chinese Optics 核心期刊

杂化偏振涡旋合成光束阵列的轨道角动量谱

杨嶒浩 程科 黄宏伟 廖赛 梁梦婷 舒凌云

Orbital-angular-momentum spectra in coherent optical vortex beam arrays with hybrid states of polarization

YANG Ceng-hao, CHENG Ke, HUANG Hong-wei, LIAO Sai, LIANG Meng-ting, SHU Ling-yun

引用本文:
杨嶒浩, 程科, 黄宏伟, 廖赛, 梁梦婷, 舒凌云. 杂化偏振涡旋合成光束阵列的轨道角动量谱[J]. 中国光学, 2023, 16(6): 1501-1511. doi: 10.37188/CO.EN-2023-0010
YANG Ceng-hao, CHENG Ke, HUANG Hong-wei, LIAO Sai, LIANG Meng-ting, SHU Ling-yun. Orbital-angular-momentum spectra in coherent optical vortex beam arrays with hybrid states of polarization[J]. *Chinese Optics*, 2023, 16(6): 1501-1511. doi: 10.37188/CO.EN-2023-0010

在线阅读 View online: https://doi.org/10.37188/CO.EN-2023-0010

文章编号 2097-1842(2023)06-1501-11

Orbital-angular-momentum spectra in coherent optical vortex beam arrays with hybrid states of polarization

YANG Ceng-hao[1], CHENG Ke[1,2*], HUANG Hong-wei[1], LIAO Sai[1], LIANG Meng-ting[1], SHU Ling-yun[1]

(1. *College of Optoelectronic Engineering*, *Chengdu University of Information Technology*, *Chengdu* 610225, *China*;
2. *Intelligent Manufacturing Industry Technology Research Institute*, *Sichuan University of Arts and Science*, *Dazhou* 635000, *China*)

* *Corresponding author*, *E-mail*: *ck@cuit.edu.cn*

Abstract: Orbital-Angular-Momentum (OAM) is one of the most important parameters in high-capacity optical communication or super-resolution imaging. Based on the Huygens-Fresnel principle and the theory of coherent combination, we propose hybridly polarized vortex beam arrays in coherent combinations of radial off-axis Gaussian beamlets with vortex and polarization Topological Charges (TC). The effect of vortex, polarization and addition TC and the number of beamlets on OAM spectra of the proposed beam arrays at input and output plane are both stressed. The results show the number of beamlet and hybrid polarization present joint effect on maximal weight of OAM-modes. An increase of maximal weight value at OAM-mode is accompanied by the growing number of the beamlet, while the hybrid polarization can not significantly increase the maximum weight of OAM spectra. As the number of beamlets increases, hybrid polarization can't significantly improve the maximal weight value in OAM spectra. Furthermore, the maximal mode equals the total TC at central Optical Vortex (OV) and it is irrelevant to the number of beamlets. Whereas for other modes for non-zero weight, their locations are jointly determined by vortex, polarization and addition TCs and the number of beamlets. This work may provide potential applications in the OAM-based communication and polarization imaging technologies.

Key words: orbital angular momentum spectrum; polarization; vortex

收稿日期:2023-05-05; **修订日期**:2023-05-26

基金项目:四川省自然科学基金项目(No. 2023NSFSC0049);智能光电系统感知及应用四川省高校重点实验室开放课题资助(No. ZNGD2202)

Supported by Natural Science Foundation of Sichuan Province (No. 2023NSFSC0049); Key Laboratories of Sensing and Application of Intelligent Optoelectronic System in Sichuan Provincial Universities (No. ZNGD2202)

杂化偏振涡旋合成光束阵列的轨道角动量谱

杨嶒浩[1], 程　科[1,2*], 黄宏伟[1], 廖　赛[1], 梁梦婷[1], 舒凌云[1]
（1. 成都信息工程大学 光电工程学院, 四川 成都 610225;
2. 四川文理学院 智能制造产业技术研究院, 四川 达州 635000）

摘要: 轨道角动量(OAM)是高容量光通信和超分辨成像技术的重要参数。利用惠更斯-菲涅尔原理和相干合成理论, 提出了杂化偏振涡旋合成光束阵列。详细研究了涡旋、偏振、附加拓扑电荷及子光束数对输入和输出平面光束的 OAM 谱的影响。结果表明: 子光束的数量和杂化偏振共同影响了 OAM 模式的最大权重, 子光束数量增加会显著提升 OAM 谱的最大权重, 但杂化偏振却不能显著提升 OAM 谱的最大权重。OAM 谱的最大模式位置总是等于光束中心光涡旋的总拓扑数, 与子光束数无关。OAM 谱所有非零权重模式的位置由涡旋、偏振、附加拓扑电荷和子光束数目共同决定。本文结果对光通信与偏振成像技术有着潜在的应用价值。

关　键　词: 轨道角动量谱; 偏振; 涡旋
中图分类号: O436.1　　**文献标志码:** A　　**doi:** 10.37188/CO.EN-2023-0010

1 Introduction

Vortex beams with helical wavefronts characterized by an azimuthal phase l (namely, vortex topological charge), e.g. Laguerre-Gaussian modes, can carry Orbital-Angular-Momentum (OAM) equivalent to $l\hbar$ per photon ($\hbar$ being reduced-Plank constant)[1, 2], which have stimulated considerable enthusiasm in optical communication, optical micromanipulation and super-resolution imaging[3-8]. Vector optical fields with hybrid states of polarization can be described by hybrid morphology with linear, circular and elliptical polarizations, and their propagations in uniaxial crystal were first studied by Milione *et al*.. in 2010[9]. Since then, many different types of hybridly polarized beams have been proposed due to their tunabilities in degree of freedom of optical polarization. For example, Gu *et al*.. investigated polarization evolution of three types of hybridly polarized beams in focal region[10], and studied the polarization rotation in a uniaxial crystal from theory to experiment[11]. The hybridly polarized beams with polarization topological charges were given by Chen *et al*.., and used to explore spin-to-orbital angular momentum conversion in near-field zone[12].

On the other hand, high-dimension or high-purity OAM spectra can be produced by the superposition of vortex beams, shape-tailored metasurfaces, a binary array of pinhole and nanosieves[13-18]. Especially, Jin *et al*.. have reported multiplexed OAMs produced by a compact phyllotaxis nanosieve. However, the effect of hybrid polarization in coherent combination on OAM-modes has not been dealt with. Can the hybridly polarized vortex beam arrays in coherent combination present pure or multiple OAM modes, and their modes can be located by mathematical method? The motivation of the present work is to explore the relation between the maximal mode of OAM spectra and total Topological Charge (TC) of central Optical Vortex (OV), and find the mathematical equations for locations of non-zero weights for all OAM-modes. The results obtained in this paper stress the effect of polarization TCs on locations of OAM-modes, which may be useful for high-capacity optical communication or super-resolution imaging.

2 OAM spectra of hybridly polarized vortex beam arrays in coherent combination

Taking the direction of z axis as the beam

propagation direction, the electric field of a single Gaussian beam with vortex and polarization TCs at the input plane of z=0 in the cylindrical coordinate system is expressed as[12, 19]

$$\boldsymbol{E}(\boldsymbol{r}_0,0)=G(\boldsymbol{r}_0)V(\boldsymbol{r}_0)\cdot [\cos(m\varphi_0+\theta)\boldsymbol{e}_x+\sin(m\varphi_0+\theta)\exp(i\delta)\boldsymbol{e}_y], \quad (1)$$

where $\boldsymbol{r}_0$=(r_0, φ_0) is the position vectors with r_0 and φ_0 being radial and azimuthal coordinates at z=0, m denotes polarization TC related to hybrid state of polarization of optical field, θ is the angle between polarization and radial direction, δ is phase retardation angle between the x_0 and y_0 components with x_0=$r_0$cosφ_0 and y_0=$r_0$sinφ_0, $\boldsymbol{e}_x$ and $\boldsymbol{e}_y$ are the unit vector along x_0 and y_0 axes, respectively. The profiles of the Gaussian beam $G(\boldsymbol{r}_0)$ and vortex core $V(\boldsymbol{r}_0)$ in Eq. (1) are described by

$$\begin{cases} G(\boldsymbol{r}_0)=\exp\left(-\boldsymbol{r}_0^2/w_0^2\right) \\ V(\boldsymbol{r}_0)=\boldsymbol{r}_0^{|l|}\exp(il\varphi_0), \end{cases} \quad (2)$$

with w_0 and l being waist width and vortex TC, respectively. From the Eqs. (1) and (2), one can see that the phase factor of electric field reduces to exp[i(m+l)φ_0] for the case of m=l, which indicates that the total TC is equal to the sum of vortex and polarization TCs, i.e. TC=m+l, at input plane of z=0. If phase retardation angle δ=0, the polarization state of optical field is linear polarization along different directions, and the optical field of m=1 can be reduced to radially or azimuthally polarized beams for θ=0 or θ=π/2, respectively. If polarization TC m=0, the polarization of optical field is not hybrid morphology, but uniformly linear, circular or elliptical polarization states.

To elucidate the OAM spectrum of beam arrays in coherent combination, we assume that it is formed with N identical off-axis beamlets with off-axis distance vector $\boldsymbol{r}_j$. The optical field of the coherent beam arrays can be written by[20]

$$\boldsymbol{E}_{\mathrm{coh}}(\boldsymbol{r}_0,0)=\sum_{j=1}^{N}\boldsymbol{E}_j(\boldsymbol{r}_0,0) \quad , \quad (3)$$

where the input jth off-axis beamlet $\boldsymbol{E}_j(\boldsymbol{r}_0,0)$=$\boldsymbol{E}(\boldsymbol{r}_0-\boldsymbol{r}_j,0)$exp(i$\phi_j$) with additional phase of ϕ_j=2π$j\eta$/N (η is additional topological charge) and the displacement vector $\boldsymbol{r}_j$=(ρcosθ_j, ρsinθ_j) with radius ρ. The propagation of the resulting beam arrays at the z plane is given as

$$\boldsymbol{E}_{\mathrm{coh}}(\boldsymbol{r},z)=\frac{k}{\mathrm{i}2\pi z}\iint\boldsymbol{E}_{\mathrm{coh}}(\boldsymbol{r}_0,0)\exp\left[\frac{\mathrm{i}k}{2z}(\boldsymbol{r}-\boldsymbol{r}_0)^2\right]\mathrm{d}\boldsymbol{r}_0, \quad (4)$$

where $\boldsymbol{r}$=(r, φ) is the position vectors at the output plane of z and k is the wave number.

The weight $\boldsymbol{R}_n$ represents the relative energy of nth OAM mode for the optical field, and its value can be calculated by

$$\boldsymbol{R}_n=\frac{\int_0^{\infty}|\boldsymbol{a}_n(r,z)|^2r\mathrm{d}r}{\sum_{n=-\infty}^{\infty}\int_0^{\infty}|\boldsymbol{a}_n(r,z)|^2r\mathrm{d}r}=\frac{P_n}{\sum_{n=-\infty}^{\infty}P_n} \quad , \quad (5)$$

with the power of OAM spectrum P_n and the expansion coefficient

$$\boldsymbol{a}_n(r,z)=\frac{1}{\sqrt{2\pi}}\int_0^{2\pi}\boldsymbol{E}_{coh}(r,\varphi,z)\exp(-in\varphi)\mathrm{d}\varphi. \quad (6)$$

Eqs. (1)-(6) provide powerful ways to solve the relative power or weight of nth OAM mode of the resulting beam arrays, where each beamlet carries vortex and polarization TCs. Although there exist the x- and y-direction polarizations of the resulting beam arrays, their OAM spectra are identical with the x and y directions in the free space. For paraxial beams, the relation among topological charge l, n-mode of OAM spectra and the weight $\boldsymbol{R}_n$ can be described by[19, 21]

$$l=\sum_{n=-\infty}^{\infty}nR_n \quad . \quad (7)$$

On the other hand, the longitudinal OAM density also provide different perspectives in the evolution of OAM, and its expression is described by[22]

$$L_z=\frac{i\varepsilon_0}{\omega}\left[E_{\mathrm{coh},x}^{*}\left(x\frac{\partial E_{\mathrm{coh},x}}{\partial y}-y\frac{\partial E_{\mathrm{coh},x}}{\partial x}\right)+E_{\mathrm{coh},y}^{*}\left(x\frac{\partial E_{\mathrm{coh},y}}{\partial y}-y\frac{\partial E_{\mathrm{coh},y}}{\partial x}\right)\right] \quad , \quad (8)$$

where ω is the circular frequency, ε_0 is the electric permittivity of a vacuum. The longitudinal OAM densities show consistency with the OAM spectra, and the relations is given by

$$L_z \propto \sum_{n=-\infty}^{\infty} nP_n \quad . \tag{9}$$

In the following numerical calculations λ=632.8 nm, w_0=1 mm, $\theta=\pi/4$, $\delta=7\pi/8$ and Rayleigh length $z_e=kw_0^2/2$ are fixed unless otherwise stated.

2.1 OAM spectra at input plane

Fig. 1 (color online) gives the OAM spectra, phases and polarization states for a single Gaussian beam with vortex and polarization TCs. It is well-known that the OAM spectrum concentrate at $n=l$ for non-polarization or uniform polarization[19] in Figs. 1 (a), 1 (d), 1 (g). However, the OAM spectra concentrate at $n=l\pm m$ in equal weight with vortex and polarization TCs at z=0 as shown in Figs. 1 (g)–1 (i). The embedded polarization TC results in the split of OAM mode. It is clear that total TCs equal $l+m$ due to spiral phase distributions in Figs. 1 (a)–1 (c), and their hybrid states of polarization improve with an increase of polarization TCs in Figs. 1 (d)–1 (f). Although the phases, polarization states and OAM spectra in a single vectorial optical fields are induced by polarization TC at the input plane, the relation of Eq.(7) still holds. For example, the power weights are both 0.5 and 0.5 at OAM-modes of n=0 and 4 for the case of (l, m)=(2, 2) in Fig. 1(i), respectively, but its spiral phase demonstrates the value of TC=4 as shown in Fig. 1(c).

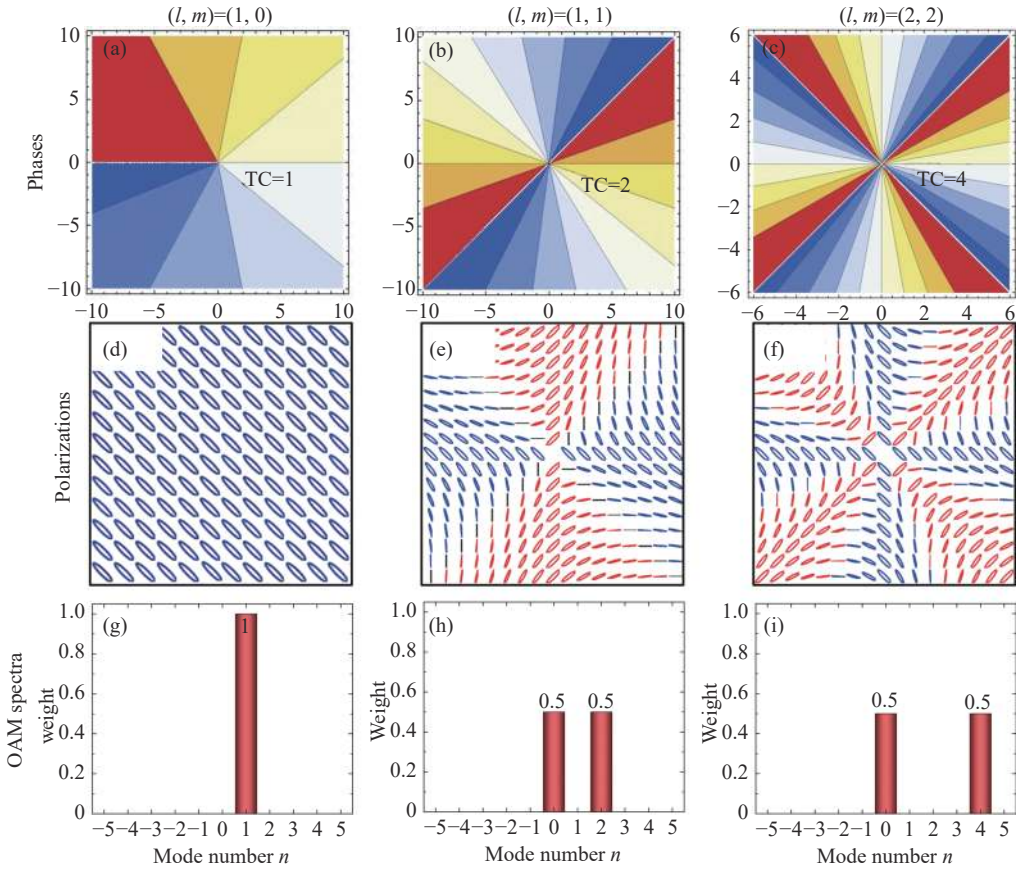

Fig. 1 Phases, polarization states and OAM spectra of a single Gaussian beam with different vortex and polarization topological charges. (a), (d), (g): (l, m)=(1, 0); (b), (e), (h): (l, m)=(1, 1); (c), (f), (i): (l, m)=(2, 2). (d), (e), (f): RH (Red) and LH (Blue) elliptical polarizations

Fig. 2 (color online) shows the OAM spectra and OAM densities of beam arrays in coherent combinations with radial, rectangular and linear symmetries at z=0, where the off-axis distances of each

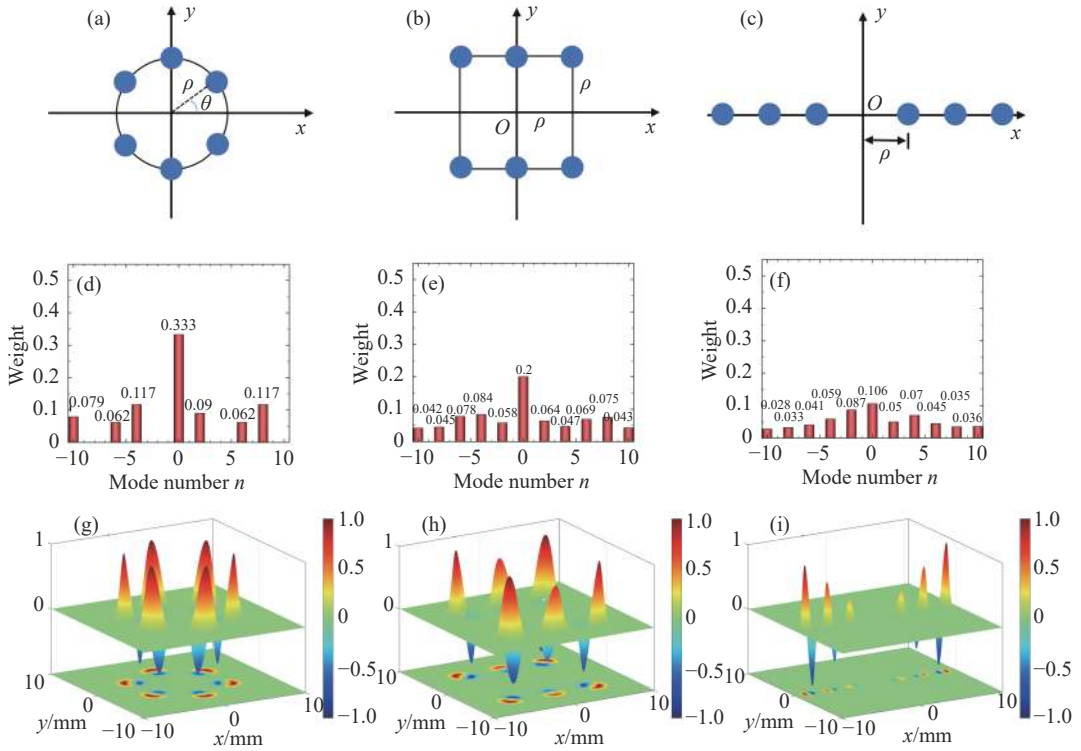

Fig. 2　The OAM spectra (d)−(f) and OAM densities (g)−(i) of beam arrays in coherent combinations with radial, rectangular and linear symmetries at z=0. (a), (d), (g): radial symmetry; (b), (e), (h): rectangular symmetry; (c), (f), (i): linear symmetry. The parameters are (l, m)=(1, 1), η=0, N=6 and ρ=5w_0

beamlet are also marked in Figs. 2 (a)−(c) and the additional topological charges are set as η=0. Comparing with the OAM-modes centered at n=0 and 2 of a single beam in Fig. 1(h), the weight values decrease from $R_{n=0}$=0.5 to 0.333 and from $R_{n=2}$=0.5 to 0.09 in Fig. 2(d). Although the relative power at mode of n=0 and 2 are suppressed, more modes appear for radial beam arrays. The maximal weigh is also found all at n=0 of OAM-mode for radial, rectangular and linear symmetries, which is due to the fact that the topological charge of central optical vortices (i.e., optical vortices at original) is zero even though there exist more non-zero vortex in the field cross section. A larger weight value at mode means that it carries more harmonic energy at this mode. The maximal weights of OAM spectra of the proposed beam arrays for different symmetry and beamlet numbers are listed in Tab. 1. As one can see, the OAM-spectra in radial symmetry present more concentrated modes than those in rectangular and linear symmetries, which means that the radial symmetry may possess relative high-quality spectra. The possible physical explanation seems to be that radial symmetry is helpful to form the expected vortex or spiral structures.

Tab. 1　The maximal weights of OAM spectra of the proposed beam arrays for different symmetry and beamlet numbers, the other parameters are the same as in Fig. 2

Symmetry	N=4	N=6	N=8
Radial	0.221	0.333	0.432
Rectangular	0.198	0.201	0.174
Linear	0.119	0.106	0.065

2.2　OAM spectra at output plane

Next, our attention is paid to the dependence of OAM-spectra in coherent combination with radial symmetry on vortex and polarization TCs (l, m), additional TC η and the number of beamlet N at the output plane. Radial beam arrays formed by N identical off-axis beamlets are depicted in Fig. 3 (a) (color online), where each beamlet at input plane

has different initial phase, i.e., $\eta\neq0$. There may exist spiral phase of central optical vortex at (0, 0, z), e.g. TC=+1, as shown in Fig. 3 (b) (color online). The OAM spectra of the corresponding beam arrays are presented in Fig. 3 (c) (color online), where the weight value $R_{n=1}$=0.92 at the maximal mode n=1. It raises the questions of whether there exist a correlation between maximal mode and central OV, and what factors determine the topological charges of central OV.

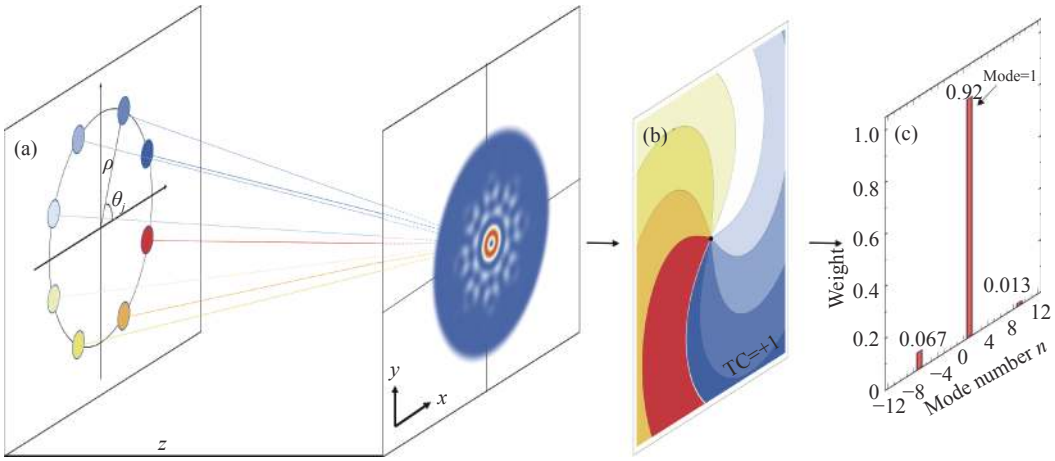

Fig. 3 (a) Illustration of center optical vortex at (0, 0, z) of beam array in coherent combination with radial symmetry at the output plane. (b) Spiral phase of center optical vortex. (c) OAM-spectra of the corresponding beam arrays. The parameters are (l, m)=(0, 0), η=+1, N=8 and $\rho=5w_0$

Fig. 4 (color online) further gives the correspondence between the topological charge of central OV and maximal modes of OAM-spectra for different l, m, η at $z=10z_e$. It is seen that the maximal mode of OAM-spectra presents a consistent one-to-one match with topological charge of central OVs, which also mean that the resulting beam arrays possess a maximal spiral harmonic power at central origin (0, 0, z). For example, the spiral phase circulating around origin of coordinates 4π in counterclockwise stand for the topological charge of TC=+2 as shown in Fig. 4 (a), then its weight of maximal mode just locating at n=2 is $R_{n=2}$=0.383. As shown in Fig. 4, the values of TC of central OVs are $l+\eta-m$ for $l+\eta\geqslant0$, while for $l+\eta<0$, the values of TC equal $l+\eta+m$. It indicates that maximal modes of OAM-spectra carrying maximal spiral harmonic powers are determined by the joint influence of vortex, polarization and additional topological charges of l, m and η. If $l+\eta\geqslant0$, the position of maximal mode is $n_{\max}=l+\eta-m$, whereas it is $n_{\max}=l+\eta+m$ if $l+\eta<0$. For example, for the case of m=1 and m=2 in Figs. 4 (c) and 4 (g), the values of TC are −1 and −2 for (l, η)=(1, −1), and their locations of maximal modes are $n_{\max}$=−1 and −2, respectively. However, for (l, η)=(0, −2), the locations are −1 and 0 in Figs. 4 (d) and 4 (h), respectively. It should be pointed out that there are plenty of optical vortices appearing at other areas, but only central OVs and maximal modes have clear correspondence.

Fig. 5 (color online) shows OAM-spectra, spiral phases of central optical vortex and OAM densities for different η at $z=10z_e$, where each beamlet at input plane possesses vortex and polarization TC of (l, m)=(1, 1). Similarly, it is found that the maximal weight of OAM spectra are centered at n=−2, −1, 1 and 2 because their locations are also determined by $n_{\max}=l+\eta+m$ for $l+\eta<0$ as shown in Fig. 5 (a). The OAM densities of beam arrays also evolve from independent side-lobes at input plane into kaleidoscope structures in far zone of $z=10z_e$ due to optical interference. The positive or negative values of OAM densities at central zones marked by dotted lines in Fig. 5 (c) agrees well with the positive or negative sign of central OVs, respectively.

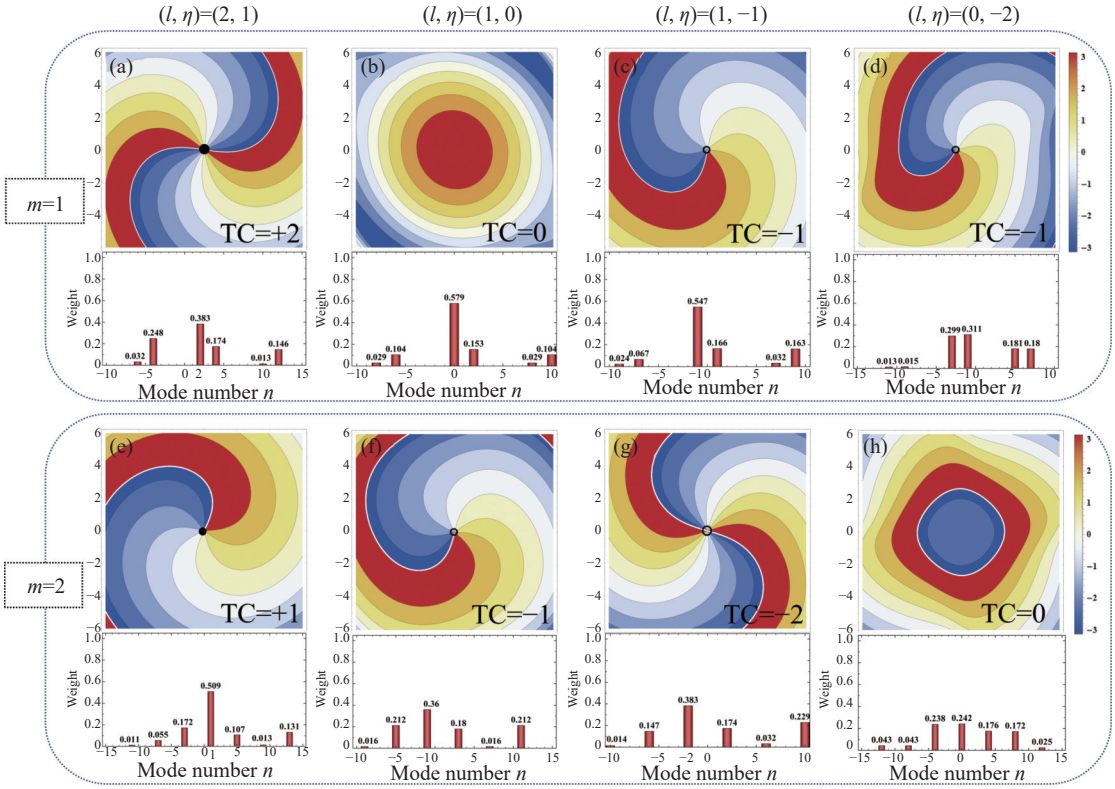

Fig. 4　The correspondence between the topological charge of central optical vortex and maximal modes of OAM-spectra for different l, m, η at $z=10z_e$. (a)−(d): $m=1$; (e)−(h): $m=2$. The parameters are $N=8$ and $\rho=3w_0$

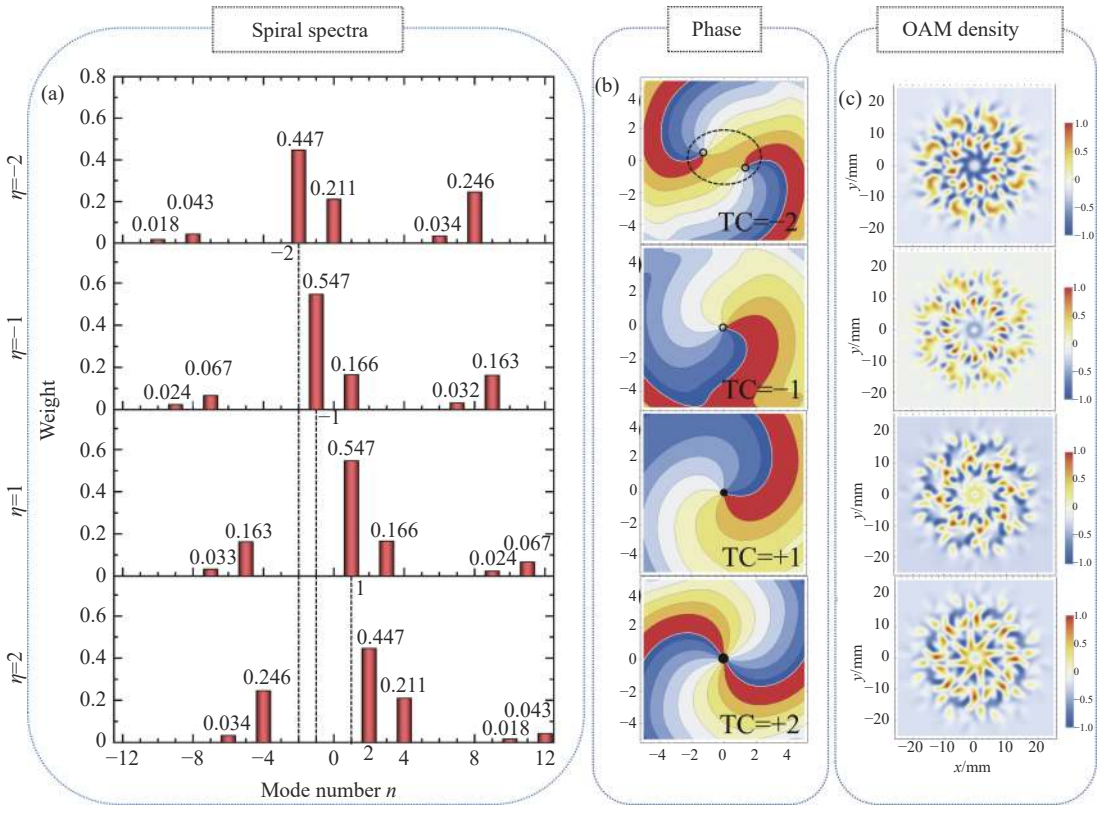

Fig. 5　OAM-spectra, spiral phases of central optical vortex and OAM densities for different η. $\eta=-2$, $\eta=-1$, $\eta=1$, and $\eta=2$ respectively, from top to bottom.The parameters are $(l, m)=(1, 1)$, $N=8$, $\rho=3w_0$ and $z=10z_e$

Now that the location of maximal mode is $n_{max}=l+\eta\pm m$, the question to raise is what happens for its maximal weight if the sum of $l+\eta$ is fixed. Fig. 6 (color online) shows the effect of polarization TCs and the number of beamlet on weight of maximal mode in OAM-spectra for a fixed $l+\eta=2$, where m=0, 1 and 2 are marked by black, red and blue lines, respectively. An increase of weight value at maximal mode is accompanied by the growing number of the beamlet, and a larger η can make larger weights. In addition, the polarization and the number of beamlet have a combined effect in maximal weight of OAM-modes. The increase of weight value in non-polarization (i.e. m=0) is more rapid than those for m=1 and m=2 with the increase of N as shown in the shaded area in Fig. 6 (a). For example, for N=7 and 12 in Fig. 6 (b) the weight improves from 0.348 to 0.917 for m=0, whereas for m=2 it only changes from 0.516 to 0.769, respectively. The results indicate that the high-purity or high-weight OAM may be obtained by increasing N or decreasing m for a fixed $l+\eta$.

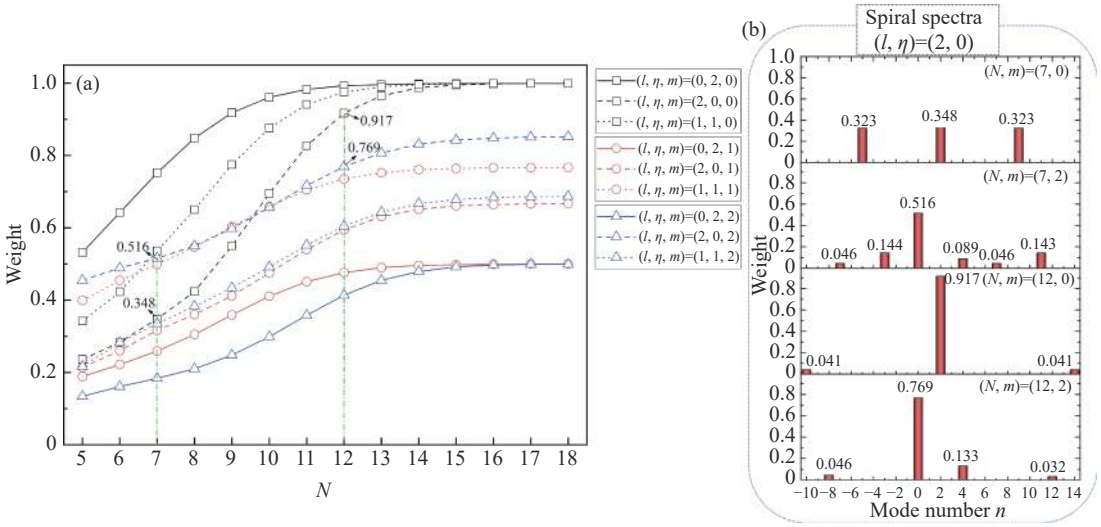

Fig. 6 (a) Effect of polarization topological charges and the number of beamlets on weight of maximal mode in OAM-spectra for a fixed $l+\eta$=2. (b) The corresponding weight in OAM-spectra for (l, η)=(2, 0). The other parameters are the same as in Fig. 5

Fig. 7 (color online) shows the locations of OAM-modes with an increase of the number of beamlet N for different l, η and m, where all non-zero modes are given. Their locations of OAM-modes gradually decrease with the growing number of beamlets, which also means that the powers at other modes disappear and transfer to a few modes. More importantly, the locations of all OAM-modes

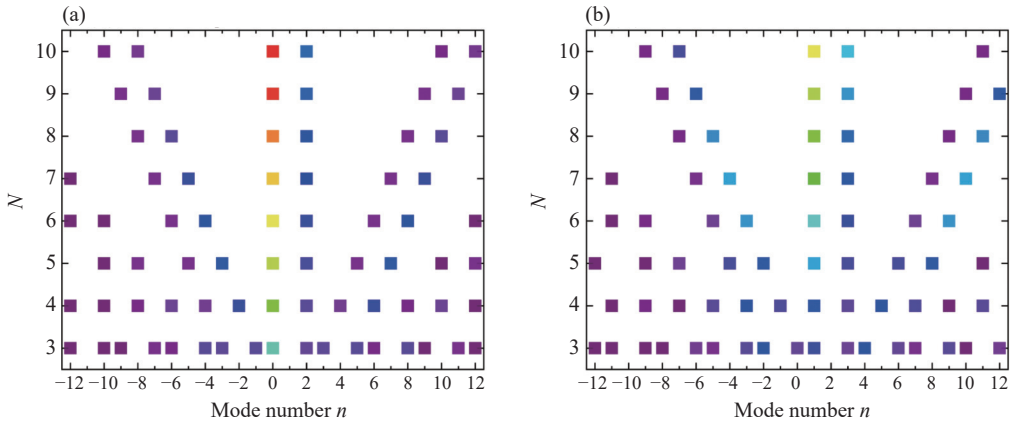

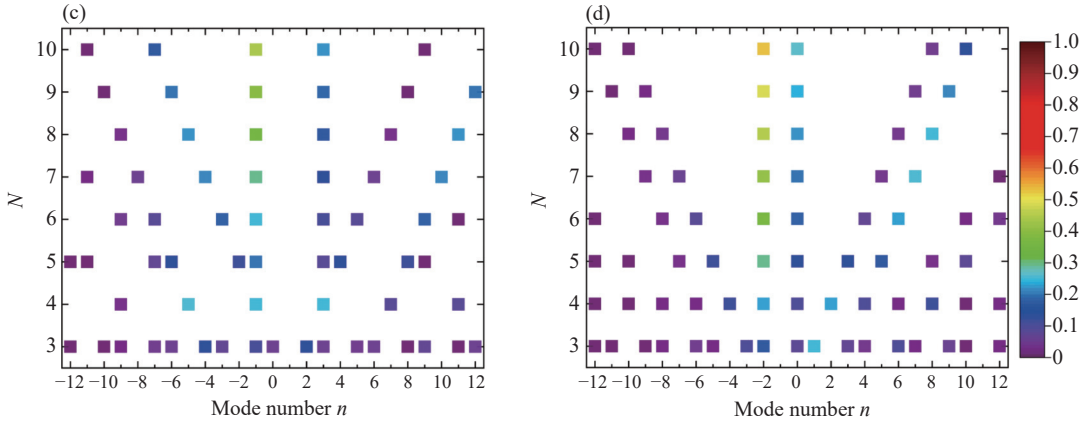

Fig. 7　Locations of non-zero weight for OAM-modes with an increasing of the number of beamlet N for different l, η and m. (a): (l, η, m)=(1, 0, 1), (b): (l, η, m)=(2, 0, 1), (c): (l, η, m)=(1, 0, 2), (d): (l, η, m)=(1, −2, 1)

for the hybridly polarized vortex beam arrays satisfy the mode equation of $n=l+\eta\pm m-\alpha N$ with arbitrary integer α (see Appendix). If $\alpha=0$, the mode reduces to $n=l+\eta\pm m$ corresponding to the case of maximal modes. For example, based on the mode equation, their locations for $N=10$ and (l, η, m)=(1, 0, 1) should are −10, −8, 0, 2, 10 and 12 if $\alpha=1$, 0 and −1, respectively, then their modes are exactly presented as shown in Fig. 7 (a). Despite their locations are plentiful, higher modes, e.g., $n=-20$, −18, 20 and 22 at $\alpha=2$ and −2, are omitted due to their extremely weak weights. These locations at other cases can be obtained by using the same method.

3　Conclusion

Hybridly polarized vortex beam arrays are proposed by the coherent combinations of N identical off-axis Gaussian beamlets with vortex and polarization topological charges, and used to explore the effect of vortex, polarization and addition topological charges (l, m, η) and the number of beamlets N on their OAM spectra. Generally, for a single beam its OAM spectrum can be induced by polarization TC, and its mode appears at $n=l\pm m$ in equal weights. However the proposed radial beam arrays present a greater concentration modes than those of rectangular and linear symmetries, which suggests that the radial beam arrays have an advantage in high-purity OAM spectra. The polarization and the number of beamlet have a combined effect on maximal weight of OAM-modes. An increase of the number of beamlets can lead to the increase of weight value at maximal mode. The hybrid polarizations caused by the embedded polarization TC not only damage the symmetry of OAM spectra, but also decrease its weight or purity at maximal modes. The maximal mode for the proposed beam arrays is equal to the total topological charge at center optical vortex, and its location is determined by $n_{\max}=l+\eta\pm m$ irrelevant to the number of beamlets. Whereas for other modes their locations appear at $n=l+\eta\pm m-\alpha N$ in connection with the number of beamlet. The proposed hybridly polarized vortex beam arrays provide potential applications in the high-capacity OAM-based communication or super-resolution imaging.

Appendix: Theoretical derivation of other non-zero OAM mode locations

According to Ref. [13], in the scalar field one can obtain the expansion coefficient in x or y-direction

$$a_n(r,z)=\frac{1}{\sqrt{2\pi}}\int_0^{2\pi}\sum_{j=1}^{N}E_j(r,\varphi,z)\exp(-in\varphi)\,\mathrm{d}\varphi. \tag{A1}$$

For simplicity, Eq. (A1) can be rewritten by letting $\theta=0$ and using Euler function as

$$a_n=\frac{1}{2\sqrt{2\pi}}(a_+ + a_-)\quad , \tag{A2}$$

with

$$a_{\pm}=\int_0^{2\pi}\sum_{j=1}^{N}E_j(r,\varphi,z)\exp\left(i\frac{2\pi j\eta}{N}\right)\cdot\exp[i(l-n)\varphi]\exp(\pm im\varphi)\mathrm{d}\varphi \quad . \tag{A3}$$

Due to the fact that each beamlet possesses the same optical fields for the radial array structures, Eq. (A3) can be expanded by using integral substitution method

$$a_{\pm}=\int_{-\frac{2\pi}{N}}^{0}E_j(r,\varphi,z)\cdot\exp[i\varphi(l\pm m-n)]\{\exp[2\pi i(l+\eta\pm m-n)/N]+\exp[4\pi i(l+\eta\pm m-n)/N]+\cdots+\exp[2\pi i(l+\eta\pm m-n)]\}\mathrm{d}\varphi \quad . \tag{A4}$$

One can consider this geometric sequence in Eq. (A4), and find it expressed as

$$\frac{1-\exp[2\pi i(l+\eta\pm m-n)]}{1-\exp[2\pi i(l+\eta\pm m-n)/N]}\approx 1 \quad . \tag{A5}$$

Only when $l+\eta\pm m-n=\alpha N$ with arbitrary integer α, which indicates that the weights of those OAM-spectra are not zero, i.e., $a_{\pm}\neq 0$, only for $n=l+\eta\pm m-\alpha N$. It should be point out that the location equation is only valid for radial array, but not applicable for the cases of rectangular and linear symmetries.

References:

[1] SHEN Y J, WANG X J, XIE ZH W, *et al*.. Optical vortices 30 years on: OAM manipulation from topological charge to multiple singularities[J]. *Light:Science & Applications*, 2019, 8(1): 90.

[2] ALLEN L, BEIJERSBERGEN M W, SPREEUW R J C, *et al*.. Orbital angular momentum of light and the transformation of Laguerre-Gaussian laser modes[J]. *Physical Review A*, 1992, 45(11): 8185-8189.

[3] BARREIRO J T, WEI T C, KWIAT P G. Beating the channel capacity limit for linear photonic superdense coding[J]. *Nature Physics*, 2008, 4(4): 282-286.

[4] WILLNER A E, PANG K, SONG H, *et al*.. Orbital angular momentum of light for communications[J]. *Applied Physics Reviews*, 2021, 8(4): 041312.

[5] EYYUBOĞLU H T. Mutual coherence function based topological charge detection in a Gaussian vortex beam optical communication system[J]. *Physica Scripta*, 2022, 97(9): 095507.

[6] GRIER D G. A revolution in optical manipulation[J]. *Nature*, 2003, 424(6950): 810-816.

[7] XIE G D, SONG H Q, ZHAO ZH, *et al*.. Using a complex optical orbital-angular-momentum spectrum to measure object parameters[J]. *Optics Letters*, 2017, 42(21): 4482-4485.

[8] WANG Y L, WANG Y ZH, GUO ZH Y. OAM radar based fast super-resolution imaging[J]. *Measurement*, 2022, 189: 110600.

[9] MILIONE G, SZTUL H I, ALFANO R R. Propagation of a hybrid vector polarization beam in a uniaxial crystal[J]. *Proceedings of SPIE*, 2010, 7613: 76130I.

[10] GU B, PAN Y, RUI G H, *et al*.. Polarization evolution characteristics of focused hybridly polarized vector fields[J]. *Applied Physics B*, 2014, 117(3): 915-926.

[11] LIAN M, GU B, ZHANG Y D, *et al*.. Polarization rotation of hybridly polarized beams in a uniaxial crystal orthogonal to the optical axis: theory and experiment[J]. *Journal of the Optical Society of America A*, 2017, 34(1): 1-6.

[12] CHEN R P, CHEW K H, DAI CH Q, *et al*.. Optical spin-to-orbital angular momentum conversion in the near field of a highly nonparaxial optical field with hybrid states of polarization[J]. *Physical Review A*, 2017, 96(5): 053862.

[13] 彭一鸣, 薛煜, 肖光宗, 等. 相干合成涡旋光束的螺旋谱分析及应用研究[J]. 物理学报, 2019, 68(21): 214206.
PENG Y M, XUE Y, XIAO G Z, *et al*.. Spiral spectrum analysis and application of coherent synthetic vortex beams[J]. *Acta Physica Sinica*, 2019, 68(21): 214206. (in Chinese).

[14] YANG Y J, ZHAO Q, LIU L L, *et al*.. Manipulation of orbital-angular-momentum spectrum using pinhole plates[J]. *Physical Review Applied*, 2019, 12(6): 064007.

[15] ZHAO Q, DONG M, BAI Y H, *et al*.. Measuring high orbital angular momentum of vortex beams with an improved multipoint interferometer[J]. *Photonics Research*, 2020, 8(5): 745-749.

[16] YANG L J, SUN SH, SHA W E I. Manipulation of orbital angular momentum spectrum using shape-tailored

metasurface[J]. *Advanced Optical Materials*, 2021, 9(2): 2001711.

[17] JIN ZH W, JANOSCHKA D, DENG J H, *et al*.. Phyllotaxis-inspired nanosieves with multiplexed orbital angular momentum[J]. *eLight*, 2021, 1(1): 5.

[18] BAI Y H, LV H R, FU X, *et al*.. Vortex beam: generation and detection of orbital angular momentum [Invited][J]. *Chinese Optics Letters*, 2022, 20(1): 012601.

[19] SHU L Y, CHENG K, LIAO S, *et al*.. Asymmetrical spiral spectra and orbital angular momentum density of non-uniformly polarized vortex beams in uniaxial crystals[J]. *Chinese Physics B*, 2023, 32(2): 024211.

[20] WANG L G, WANG L Q, ZHU SH Y. Formation of optical vortices using coherent laser beam arrays[J]. *Optics Communications*, 2009, 282(6): 1088-1094.

[21] KOTLYAR V V, KOVALEV A A. Optical vortex beams with a symmetric and almost symmetric OAM spectrum[J]. *Journal of the Optical Society of America A*, 2021, 38(9): 1276-1283.

[22] TORNER L, TORRES J P, CARRASCO S. Digital spiral imaging[J]. *Optics Express*, 2005, 13(3): 873-881.

Author Biographics:

Yang Ceng-hao (1999—), male, was born in Mian yang, Sichuan province, M. Phil, College of Optoelectronic Engineering, Chengdu University of Information Technology. His research interests are on propagation and control of High-Power Lasers. E-mail: scaxych@163.com

Cheng Ke (1979—), male, was born in Jianli, Hubei province, Ph.D., Professor, College of Optoelectronic Engineering, Chengdu University of Information Technology. His research interests are on propagation and control of High-Power Lasers. E-mail: ck@cuit.edu.cn